Computers and Concrete, *Vol. 32, No. 5 (2023) 487-498*
https://doi.org/10.12989/cac.2023.32.5.487

Flexural behavior of reinforced concrete beams strengthened with an ultra-high performance concrete panel of various thicknesses

Seonhyeok Kim[1], Taegeon Kil[1], Sangmin Shin[2], Daeik Jang[1], H.N. Yoon[1,3,4], Jin-Ho Bae[1], Joonho Seo*[1,3] and Beomjoo Yang**[5]

[1]*Department of Civil and Environmental Engineering, Korea Advanced Institute of Science and Technology, 291 Daehak-ro, Yuseong-gu, Daejeon 34141, Republic of Korea*
[2]*Korea Institute of Civil Engineering and Building Technology, 283 Goyangdae-ro, Ilsanseo-gu, Goyang-si, Gyeonggi-do, 10223, Republic of Korea*
[3]*Applied Science Research Institute, Korea Advanced Institute of Science and Technology, 291 Daehak-ro, Yuseong-gu, Daejeon 34141, Republic of Korea*
[4]*Construction Safety Research Institute, Korea Testing and Research Institute, 68 Gajaeul-ro, Seo-gu, Incheon 22829, Republic of Korea*
[5]*School of Civil Engineering, Chungbuk National University, 1 Chungdae-ro, Seowon-gu, Cheongju, Chungbuk 28644, Republic of Korea*

(*Received November 7 2022, Revised June 27, 2023, Accepted July 5, 2023*)

Abstract. The present study investigated the flexural behavior of reinforced concrete (RC) beams strengthened with an ultra-high performance concrete (UHPC) panel having various thicknesses. Two fabrication methods were introduced in this study; one was the direct casting of UHPC onto the bottom surface of the RC beams (I-series), and the other was the attachment of a prefabricated UHPC panel using an adhesive (E-series). UHPC panels having thicknesses of 10, 30, 50, and 70 mm were applied to RC beams, and these specimens were subjected to four-point loading to assess the effect of the UHPC thickness on the flexural strengthening of RC beams. The test results indicated that the peak strength and initial stiffness were vastly enhanced with an increase in the thickness of the UHPC panel, showing an improved energy dissipation capacity. In particular, the peak strength of the E-series specimens was higher than that of I-series specimens, showing high compatibility between the RC beam and the UHPC panel. The experimental test results were comparatively explored with a discussion of numerical analysis. Numerical analysis results showed that the predictions are in fair agreement with experimental results.

Keywords: finite element method; flexural behavior; reinforced concrete; strengthening; ultra-high performance concrete

1. Introduction

Reinforced concrete (RC) is one of the most widely used materials in the construction sector. RC structures must perform the designed functions during their service lifetimes. However, these structures are inevitably exposed to deterioration caused by the external environment in which they are applied, such as repeated and excessive loads, corrosion of the steel reinforcement by carbonation, and freeze-thaw cycles (Manfredi and Pecce 1997, Deng 2005, Murthy *et al.* 2018a). These conditions can severely weaken the properties of RC structures. To recover the load-carrying capacity, serviceability, and mechanical properties of aged RC structures, they should be treated with proper retrofitting or strengthening measures.

Various methods have been used for the retrofitting or strengthening of aged RC structures. Fiber-reinforced plastic (FRP) and carbon fiber-reinforced plastic (CFRP) laminates are among the most commonly used materials to strengthen existing RC structures due to their high strength, high stiffness-to-weight ratio, and good corrosion resistance (Buyukozturk and Hearing 1998, Spadea *et al.* 1998, Toutanji *et al.* 2006, Murthy *et al.* 2018a). RC structures strengthened with these laminates exhibit enhanced flexural strength and stiffness according to earlier findings (Buyukozturk and Hearing 1998, Lee and Hausmann 2004, Toutanji *et al.* 2006, El-Enein *et al.* 2014).

In addition, numerous analytical studies have been conducted to enhance our understanding of the strengthening effects when using these materials on RC structures (El-Mihilmy and Tedesco 2000, Monti and Liotta 2005, Wenwei and Guo 2006). However, these methods have limitations, which can in turn lead to brittle failures without appreciable deformation due to discrepancies in the tensile strength and/or stiffness between FRP or CFRP laminates and concrete (Attari *et al.* 2012, Murthy *et al.* 2018b). This issue has motivated the development of retrofitting strategies utilizing cementitious materials to maintain compatibility with existing RC structures.

Ultra-high performance concrete (UHPC), a cement-based composite, has superior mechanical properties in comparison with those of normal or high-strength concrete. In particular, UHPC shows greater compressive strength by

*Corresponding author, Ph.D.
E-mail: junhoo11@kaist.ac.kr
**Corresponding author, Ph.D.
E-mail: byang@cbnu.ac.kr

ISSN: 1598-8198 (Print), 1598-818X (Online)

two to three times and greater flexural strength by as much as six times compared to those of high-strength concrete (Lubbers 2003). Furthermore, UHPC has an extremely high packing density and low porosity (Lee *et al.* 2018), enhancing its low permeability, diffusivity, and sorptivity (Yalçınkaya and Yazıcı 2017, Haile *et al.* 2019). Owing to these advantages, UHPC is considered as a viable alternative capable of mitigating the abovementioned drawbacks of FRP and CFRP laminates (Al-Osta *et al.* 2017, Murthy *et al.* 2018a).

Numerous studies have investigated the performance of RC structures strengthened with UHPC as a potential retrofitting method (Hussein and Amleh 2015, Murthy *et al.* 2018a, Murthy *et al.* 2018b). Hussein and Amleh (Hussein and Amleh 2015) reported that an RC beam fabricated using normal or high-strength concrete with ultra-high performance fiber-reinforced concrete cast under tension showed enhanced flexural and shear capacities. Murthy *et al.* (Murthy *et al.* 2018b) reported that damaged RC beams could be successfully fortified and rehabilitated when strengthened with UHPC strips. Other studies investigated the potential of utilizing UHPC as a strengthening material given that this method can enhance or recover the load-carrying capacity, serviceability, and mechanical properties of damaged RC structures. However, a comprehensive investigation of the RC beam strengthened UHPC panels of various thicknesses to identify and predict the flexural behavior of these concrete has not been conducted. In particular, the effects of the thickness of UHPC as a strengthening material and the effects of the attachment method used on the flexural behavior of RC beams were not included in the scope of earlier works.

The present paper, therefore, investigates the effect of the thickness of the UHPC panel and strengthening method used on the flexural behavior of the RC beams strengthened with a UHPC, as this material has been attracting attention as an alternative to FRP and CFRP laminates. The flexural behavior of the RC beam strengthened with UHPC was explored by investigating the failure mode, load-deflection capabilities, and load-strain behavior. Furthermore, a numerical analysis using the nonlinear finite element analysis method was carried out to predict the flexural strengthening effect of the RC beams strengthened with a UHPC, and the results were compared with those from an experiment.

2. Experimental program

2.1 RC beam specimens preparation

The concrete mixture here was composed of Type I Portland cement, sand (river sand), and gravel (maximum size of 18 mm). The mixture proportion of the concrete is tabulated in Table 1. The mixture of Portland cement, sand, and gravel was dry mixed for 10 min using a concrete pan mixer. Shortly afterward, the mixture was further mixed with water for 10 min and was cast into designated molds with the aid of a mechanical vibrator.

The concrete slump value after mixing, measured in accordance with ASTM C143/C143M, was 200 mm (ASTM-C143 2015). The fresh concrete was cured under ambient conditions. The compressive strength of the concrete after 28 days of curing was 33.4 MPa. Deformed steel bars (rebars) with diameters of 10 mm were used for longitudinal reinforcement of the RC beams. The yield stress of the rebar was 450 MPa and the elastic modulus was 210,000 MPa.

Table 1 Mixture proportion of the concrete (kg/m^3)

Cement	Sand	Gravel	Water
385.0	782.0	954.0	192.5

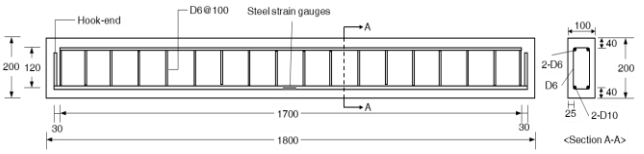

Fig. 1 Details of the RC beams

Table 2 Chemical composition of the binder materials used in this study

(wt %)	CaO	SiO_2	Al_2O_3	Fe_2O_3	SO_3	MgO	K_2O	Na_2O	LOI*
Cement	62.5	21.0	5.9	3.2	2.1	-	-	-	3.2
Silica fume	0.1	96.8	0.1	0.8	-	0.2	0.4	0.1	1.5

*Loss-on-ignition

A total of nine RC beams with identical dimensions and reinforcements were fabricated. One RC beam without any treatment was used as the control specimen, and the rest eight RC beams were used for strengthening tests in accordance with designated strengthening thickness and method. The details of the RC beams are illustrated in Fig. 1. The dimensions of the RC beams were 1,800 mm (length)×100 mm (width)×200 mm (depth). The RC beams were designed to exhibit a flexural failure, i.e., the beams were under-reinforced (Gil-Martina and Hernandez-Montes 2021). Two D10 rebars were used as a type of longitudinal reinforcement. In addition, D6 bars (stirrups) were vertically arranged along the beam to meet the minimum shear reinforcement ratio requirement. Two D6 bars at the top of the beam served only as a hanger for the arrangement of the stirrups, meaning that they were not taken into account in the analysis. Each end of the longitudinal rebars was bent to form a hook-like shape in order to prevent the direct pull-out phenomenon of the rebars during loading.

2.2 Properties of UHPC for strengthening

Type I Portland cement and silica fume were introduced as binder materials. The chemical composition of the binder materials is provided in Table 2. Quartz sand having a particle size in the range of 0.17 - 0.7 mm was included as an aggregate. Silica powder was incorporated as a micro-filler. In addition, an expansive agent (EA) based on calcium sulfoaluminate (CSA) and an autogenous shrinkage reducer (ASR) were used to alleviate the volumetric

Table 3 Mixture proportion of the UHPC as expressed in terms of the mass ratio

Cement	Silica fume	Silica powder	Sand	CSA-EA	Water	SP	ASR	SF
1.00	0.22	0.33	1.10	20 kg/m^3	0.21	0.04	0.01	2 vol.%

Table 4 Mechanical properties of UHPC for strengthening

Mechanical properties	Value (MPa)	Method
Compressive strength	140	ASTM C39/C39M 2021
Flexural strength	23	ASTM C348 2021
Splitting tensile strength	26	ASTM C496 2017
Modulus of elasticity	53,415.51	ASTM C469 2021

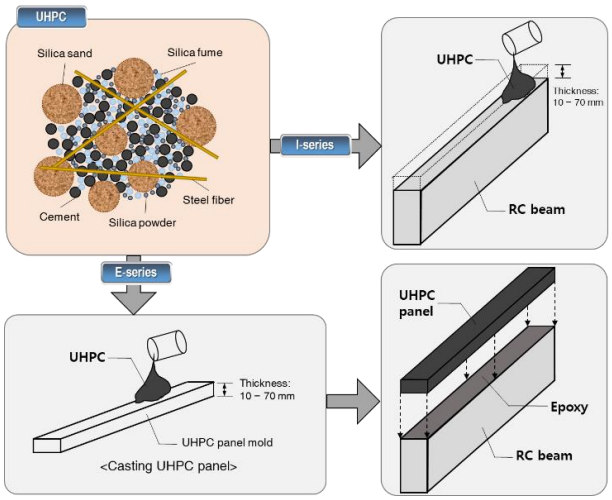

Fig. 2 Schematic illustration of the strengthening method

reduction during the curing process. Steel fiber (SF) with a diameter and length of 0.2 mm and 13 mm, respectively, was also used. A polycarboxylate-based superplasticizer (SP) was used to achieve a water-to-binder ratio of 0.17 with proper workability.

The mixture proportion of the UHPC as expressed in terms of the mass ratio is shown in Table 3. The powders were mixed for 10 min using a concrete pan mixer, and this was followed by 10 min of wet mixing. The flowability value as measured in accordance with ASTM C1437 exceeded 200 mm (ASTM-C1437 2020). The slurry was then poured either into the designated panel molds or directly onto the bottom surface of the RC beams. Panel molds having a fixed length and width of 1,800 mm and 100 mm, respectively, with various thicknesses of 10 mm, 30 mm, 50 mm, and 70 mm were used. The mechanical properties of the UHPC were assessed by measuring the compressive strength, flexural strength, splitting tensile strength, and modulus of elasticity, which are tabulated in Table 4. All mechanical properties of UHPC were measured on the day identical to the RC beam flexural testing day. Note that the cubic samples was used in this paper for the compressive strength measurement due to the limitation of load capacity of universal testing machine, though ASTM associated with the test uses cylinder samples. In addition, the splitting tensile strength was determined using the first peak load because an increase in the load beyond the first peak load is not attributed to the actual splitting tensile strength of the UHPC but to an increase in the surface area because the UHPC was crushed.

2.3 Strengthening method and curing regimes

Two strengthening methods were adopted in this study (Fig. 2.). The first was the direct casting of UHPC onto the bottom surface of the RC beams (I-series). The second was to attach UHPC panel onto the bottom surfaces of the RC beams using a commercial concrete adhesive (E-series). Details of the strengthening method of E-series are provided later in this section. The former method is free from complexity in the procedure, while the latter may be useful at sites where the cast-in-place approach for UHPC is not available.

The UHPC was cast after 28 days of RC beam curing. The UHPC was cured under ambient conditions for one day, followed by a three-day steam curing treatment using steam generators. A schematic illustration of the steam curing setup is displayed in Fig. 3. It is important to note that the separators shown in Fig. 3 were applied to minimize the effect of the elevated temperature on the properties of the RC beams, as this effect can influence the properties of the adjacent RC beam. The average internal temperature, as measured by thermocouples, was maintained at 70 ºC during the steam curing process. After the steam curing process, the UHPC panels were attached to the RC beams using a commercial new/old concrete adhesive. An adhesive

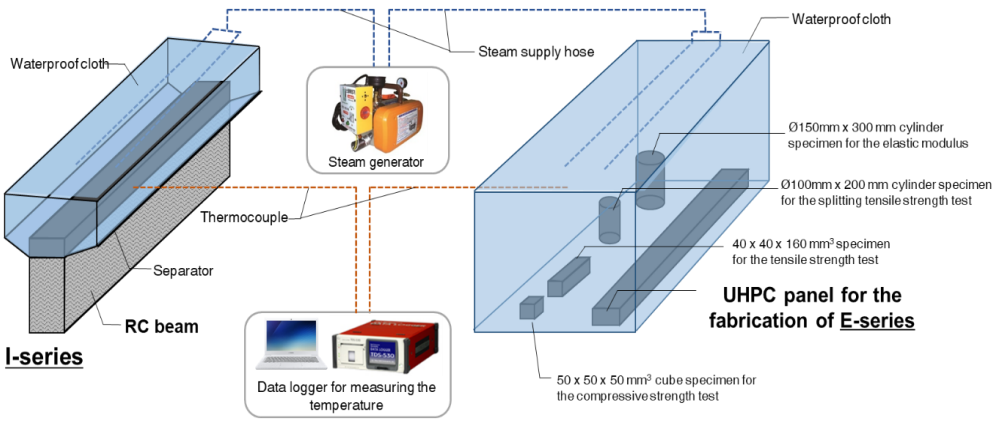

Fig. 3 Schematic illustration of the steam curing setup

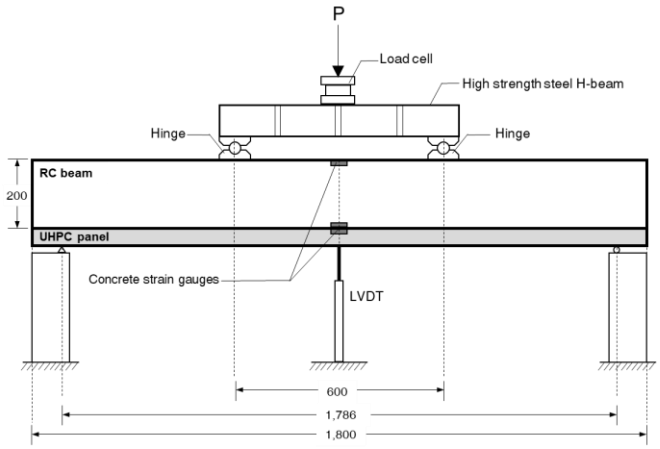

Fig. 4 Schematic illustration of test setup of RC beams strengthened with UHPC

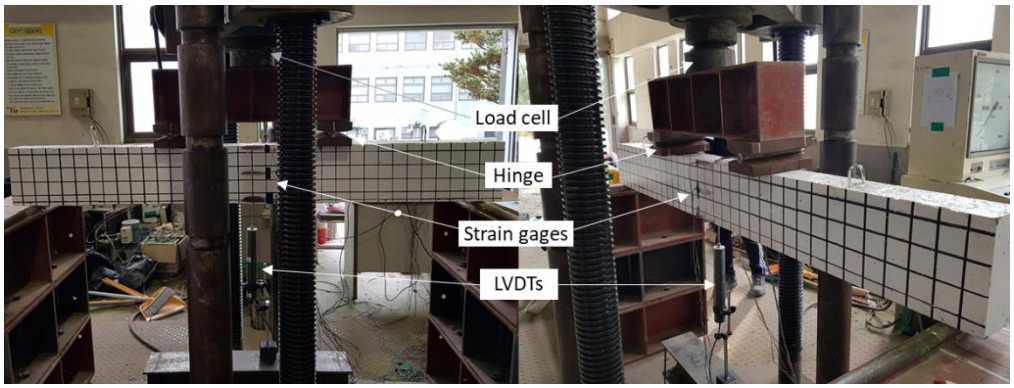

Fig. 5 Test setup of RC beams strengthened with UHPC

with compressive strength of 50 MPa, tensile strength of 18.5 MPa, and adhesion strength of 10 MPa, provided by the manufacturer (BOWTEK Carobonex Co. Ltd., South Korea), was used. All specimens were then cured further for 25 days under ambient conditions.

Note that the specimens were labeled depending on their casting method and strengthened thickness, i.e., the I30 specimen represents an RC beam strengthened with UHPC having a thickness of 30 mm created by means of direct casting, while the E50 specimen indicates an RC beam strengthened with the precast UHPC panel having a thickness of 50 mm.

2.4 Test details

Schematic illustration of test setup and test set up of the RC beams strengthened with UHPC are shown in Figs. 4 and 5. For this experiment, a single specimen was used for each thickness and series. The beams were tested under four-point loading with a constant loading rate of 0.01 mm/s. A linear variable differential transformers (LVDTs) was placed in the middle of the beam to measure the displacement at the midspan point. Concrete strain gauges were attached onto the top and bottom fibers in the mid-span area. A concrete strain gauge was also attached to the

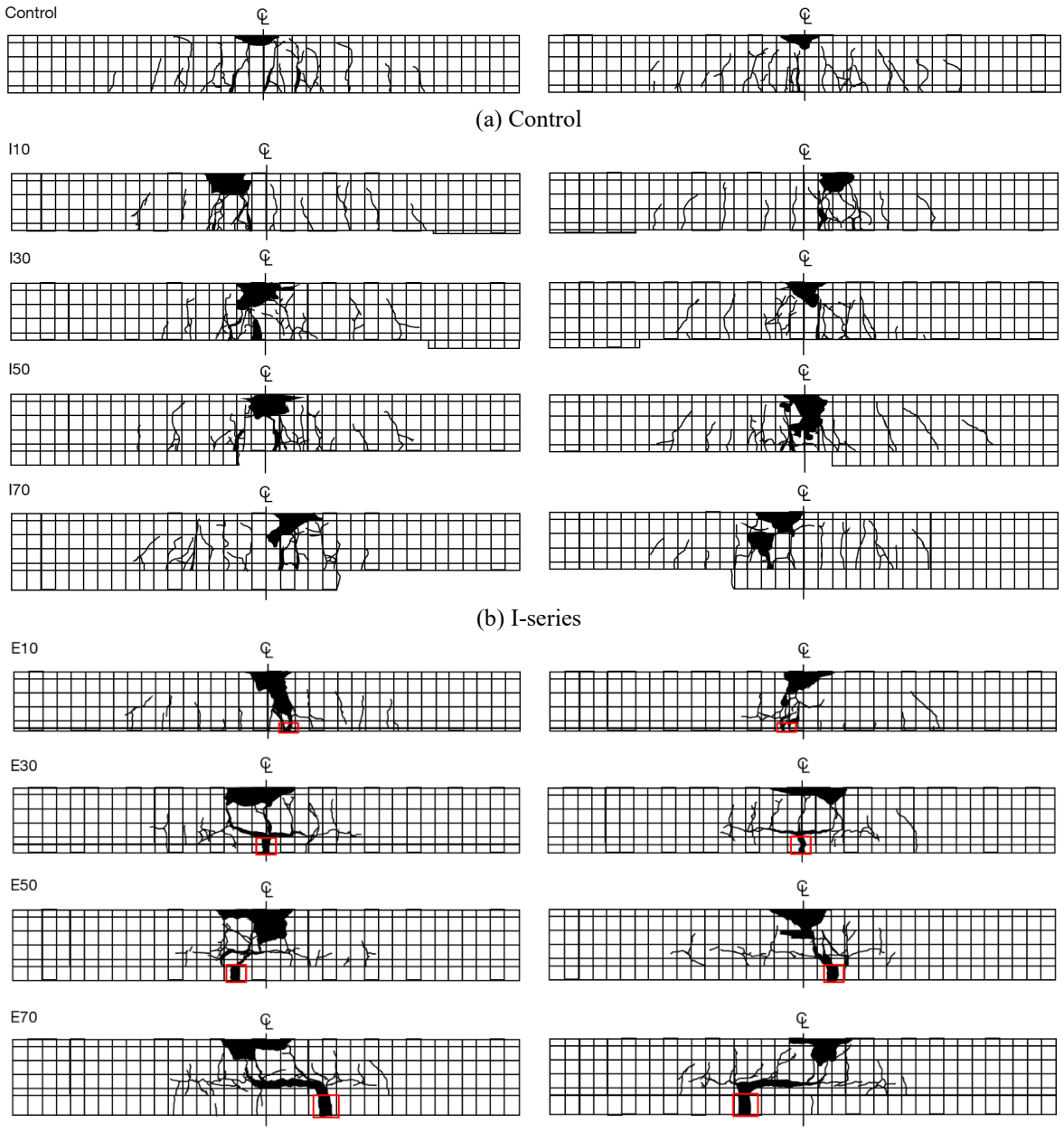

Fig. 6 Failure mode and crack pattern of the (a) Control, (b) I-series and (c) E-series specimens (Squared regions indicate a disconnection of the UHPC panel.)

top of the UHPC panel to evaluate the interfacial behavior and compatibility between the RC beam and the UHPC panel. Steel strain gauges were attached to the rebars in the mid-span area prior to casting in order to monitor the deflection of the rebars.

3. RC beam test results

3.1 Crack pattern and failure model

The failure mode and crack pattern of the RC beam strengthened with UHPC are shown in Figs. 6.and 7. The crack pattern of a control specimen provided evidence of a flexural failure, during which vertical cracks initiated from the bottom side of the midspan area and propagated toward both ends of the beam as the load was increased (Kassem *et al.* 2011, Al-Osta *et al.* 2017). The I-series specimens showed a crack pattern similar to that of the control specimen. The crack pattern of the I-series specimens exhibited vertical cracks mainly centered in the mid-span area with several inclined flexural-shear cracks (Theriault and Benmokrane 1998). The vertical cracks in the I-series specimens were more concentrated at the mid-span of the specimen as the thickness of the UHPC panel increased. The distance from the far left crack to the far right crack of the I10 specimen was 1,005 mm, and this value decreased to 837.5 mm for the I70 specimen. It should be noted that

(a) Control

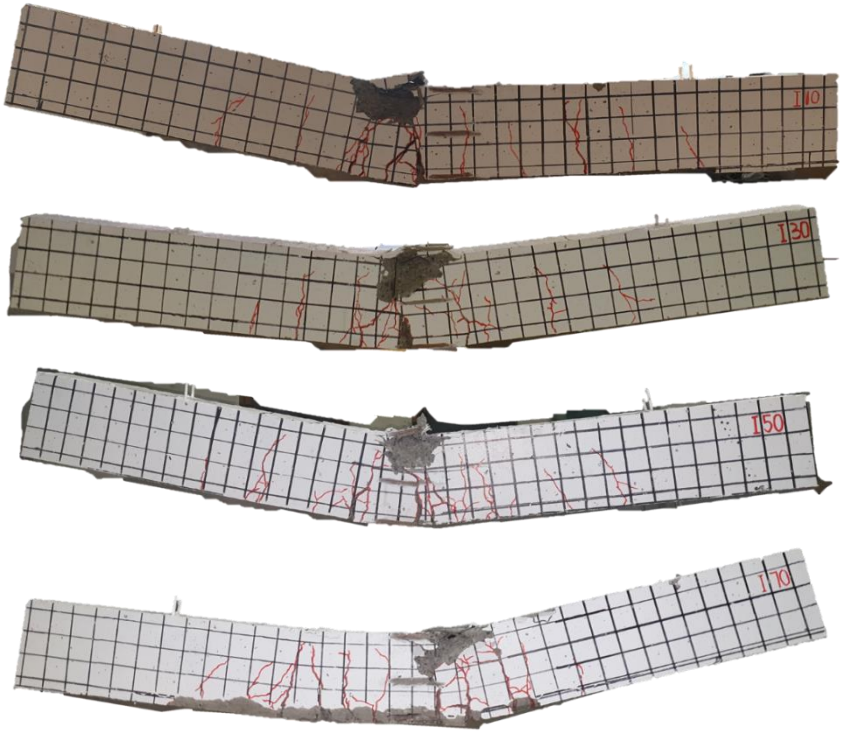

(b) I-series

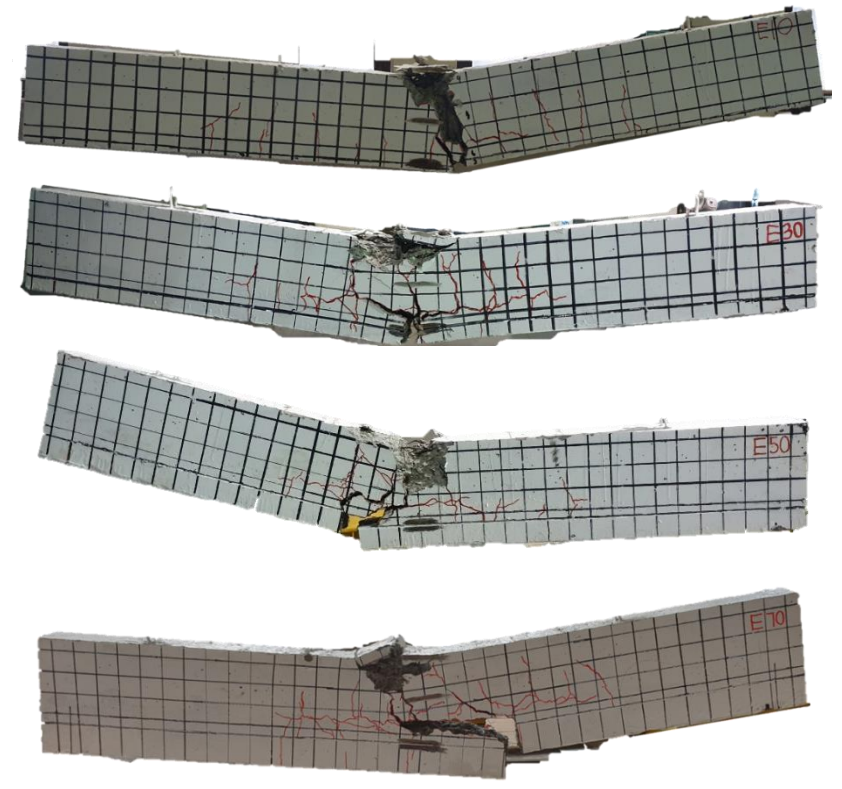

(c) E-series

Fig. 7 Failure mode and crack pattern of the (a) Control, (b) I-series and (c) E-series specimens

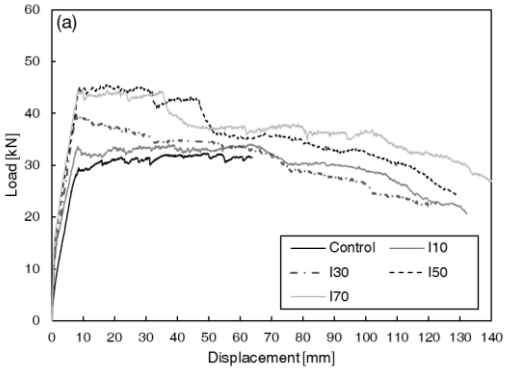

(a) I-series

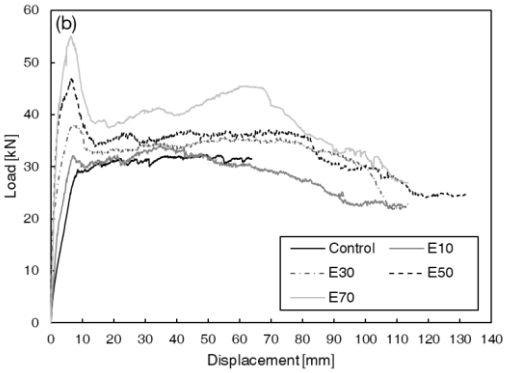

(b) E-series

Fig. 8 Load-deflection curve of the (a) I-series and (b) E-series specimens with the control specimen

all I-series specimens underwent detachment of the UHPC panel from the RC beam as shown in Fig. 7(b), presumably due to the low adhesion strength between the RC beam and the UHPC panel. Overall, crack growth was not observed on the UHPC panel, though for this panel, direct detachment from the RC beam was noted, which can cause damage to the environment underneath via the abrupt plunge of the UHPC fractures when subjected to an excessive load.

The crack pattern of the E10 specimen was similar to that of the control and the I10 specimens, meaning that the UHPC panel having a thickness of 10 mm has a limited effect on the flexural performance of the RC beam. The detailed flexural behavior of the E10 specimen is discussed in the following section. However, the crack patterns of the E30, E50, and E70 specimens showed different aspects of crack propagation as compared to those found in other specimens. The UHPC panels became disconnected upon the initiation of the growth of major cracks centered at the mid-span of the RC beam. In addition, the propagation of vertical cracks resulted in the formation of horizontal cracks connected to the vertical cracks. It is interesting to note that several cracks were observable on the UHPC panels of the E-series specimens, whereas these cracks were not identified on those panels of the I-series specimens, indicating that the UHPC panels of the E-series specimens could more efficiently carry the load and dissipate the energy due to the enhanced adhesion between the panel and the RC beam.

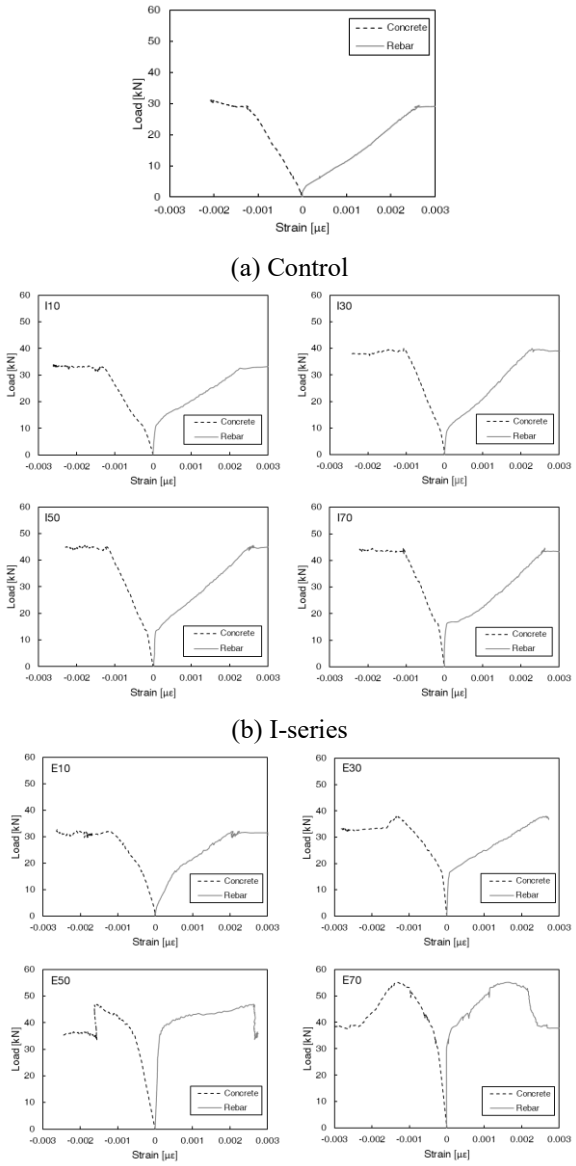

(a) Control

(b) I-series

(c) E-series

Fig. 9 Load-strain of rebar and top of the RC beam of the (a) Control, (b) I-series and (c) E-series specimens

3.2 Load-deflection

The load-deflection curve of the RC beam strengthened with UHPC is shown in Fig. 8. The load-deflection curve of the control specimen showed typical flexural behavior of RC beams. The load increased linearly up to approximately 30 kN, at which the rebars started to yield. Thereafter, the load was maintained upon further loading up to the fracture point. For the I-series specimens, the peak strength of the beam increased with an increase in the thickness of the UHPC panel, yet the I50 and I70 specimens showed similar peak loads. The increase rates of the peak strength levels of the I10, I30, I50, and I70 specimens as compared to that of the control specimen were 14.08%, 33.94%, 54.53%, and 54.34%, respectively. A slow reduction in the load was observed in the I50 and I70 specimens at the deflection level of 30-40 mm, after which concrete crushing occurred.

The E-series specimens showed a different type of load-deflection behavior. They showed a drastic increase in the load with a small amount of deflection as compared to the I-series specimens. The peak load increased as the thickness of the UHPC panel increased. The rates of increase of the peak load of the E10, E30, E50, and E70 specimens as compared to that of the control specimen were 7.66%, 31.50%, 62.13%, and 90.51%, respectively, showing higher efficiency than the I-series specimens. Thereafter, a rapid load decrease was observed after the peak load was reached, with the pull-out of steel fibers observed in the UHPC. The contribution of UHPC at the tensile area, which acted as the main reinforcement, was reduced as the pull-out of the steel fiber commenced (Bang *et al* 2022). The E10 specimen showed no specific increase in the peak load. The peak loads of E50 and E70 specimens were higher than those of the I50 and I70 specimens, an outcome associated with the high adhesion strength between the RC beam and the UHPC panel. It should be noted that the initial stiffness of the specimen increased with an increase in the UHPC thickness and was more notable in the E-series specimens than in the I-series specimens.

3.3 Load-strain behavior

The load-strain curve of the RC beam strengthened with UHPC is shown in Fig. 9. Fig. 9 illustrates the correlation between the rebar and the concrete strain values, each measured on the rebar and top surface of the mid-span area of the specimens. The rebar yielded in all specimens regardless of the thickness of the UHPC, indicating that a flexural failure occurred even in the specimens strengthened with UHPC. Despite the yield of the rebar, the peak strength increased in both the I- and E-series specimens in comparison with the control specimen. The peak strength of the I-series specimens increased as the thickness of the UHPC panel increased, and there was no increase in the load after the rebar yielded. The load capacity of the E-series specimens was enhanced as the thickness of the UHPC panel was increased, while the load-strain curves of the E-series specimens showed a different aspect, particularly for the E50 and E70 specimens, which indicated a clearly contrasting eature from those of the other specimens. The rebar and concrete strain were nearly unaltered with a rapidly increasing load due to the straining effect by the UHPC panel, which ultimately resulted in an increase in the peak load. The drastic decrease in the load found in the E50 and E70 specimens is associated with the tensile failure of the UHPC panel (disconnection, see Fig. 6(c)). Fig. 10 displays the strain of the bottom surface of the RC beam and the UHPC panel. Comparing these two strain values allows one to determine the compatibility between the UHPC panel and the RC beam.

It should be noted that the detachment of the UHPC panel from the RC beams was noted in the I-series specimens, leading to the occurrence of slip at early loading, with the strain gauges severely damaged during loading. Due to this phenomenon, the strain values of the I-series specimens were not obtained, except for the I10 specimen. The significant discrepancy in the strain values in the I10 specimen (Fig. 10(b)) is evidence of some incompatibility that occurred during loading. Meanwhile, the E-series specimens with high adhesion between the RC beam and the UHPC panel showed nearly identical strain values during loading.

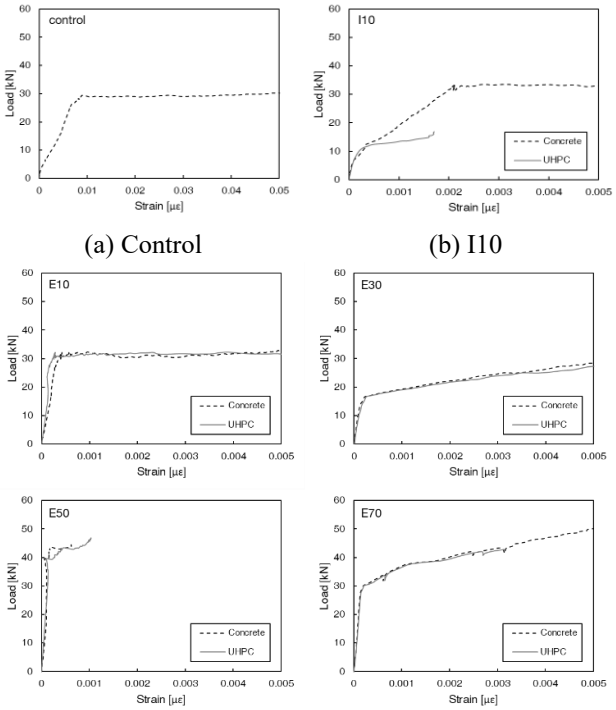

(a) Control (b) I10

(c) E-series

Fig. 10 Load-strain of the bottom of the RC beam and the UHPC-reinforcement of the (a) Control, (b) I10 and (c) E-series specimens

Table 5 Elastic properties of concrete and UHPC (Al-Osta *et al*. 2017)

Property	Concrete	UHPC
Modulus of elasticity (MPa)	29,000	53,416
Poisson's ratio	0.18	0.15

4. Numerical analysis

A numerical analysis was conducted via a nonlinear finite element analysis to predict the flexural strengthening effect of the RC beam strengthened with UHPC panels having various thicknesses. The commercially available software ABAQUS (ABAQUS/CAE 6.13 version) was used to model the flexural behavior of the specimens. The values of modulus of elasticity were obtained from our experimental results in Section 2.2 and the Poisson's ratio values were referenced from Al-Osta *et al.* (2017) (Table 5). The nonlinear behavior of the tested beam specimens was modeled using the concrete damage-plasticity (CDP) model available in ABAQUS.

The CDP model contains the combination of isotropic damaged elasticity and non-associated hardening plasticity

Table 6 Concrete damage plasticity model parameters for concrete and UHPC (Lee and Fenves 1998, Al-Osta *et al.* 2017)

	Ψ*	ε*	fb0/fc0	K	Viscosity parameter
Concrete	36	0.1	1.16	0.667	0
UHPC	36	0.1	1.16	0.667	0

* Ψ=Dilation angle [degrees], ε=Eccentricity

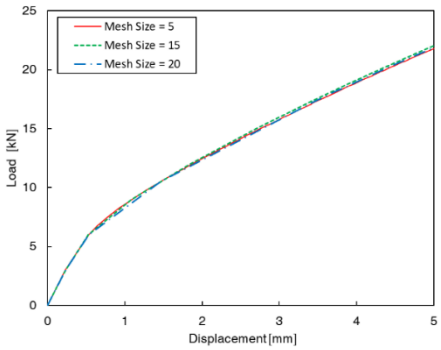

Fig. 11 Simulated load-displacement behaviors of control specimens to different global mesh size

to consider the irreversible damage happened during the fracturing procedure (ABAQUS 2013, Choi *et al.* 2022). The CDP model adopts the yield function, as derived by Lubliner *et al.* (1989) and Lee and Fenves (1998), to account for different evolution of strength under compression and tension (ABAQUS 2013). The simulation of all load-displacement behaviors was stopped at the structural failure in the CDP model (Murthy *et al.* 2018b, Al-Osta *et al.* 2017). The details of the formulations of the CDP model can be found in Lubliner *et al.* (1989) and Lee and Fenves (1998).

It should be noted that the CDP model parameters input in the present study are tabulated in Table 6, referenced from Lubliner *et al.* (1989) and Al-Osta *et al.* (2017). In addition, yield stress and modulus of elasticity values of 450 MPa and 210,000 MPa, respectively, were used to simulate the rebar according to an elastic-perfectly plastic relationship (Al-Osta *et al.* 2017). Furthermore, the material parameters utilized in the present simulation were assumed by referring to the outcomes reported in the previous works. Nevertheless, it is important to highlight that conducting relevant experimental investigations to determine the precise values of these parameters is necessary for achieving more accurate and realistic predictions in the present simulation.

Over the years, several researchers have proposed theoretical modeling approaches for simulating discrete cracks in concrete using finite element analysis (Rabczuk *et al.* 2004, 2007, 2010, 2008, Hamdia *et al.* 2017). Rabczuk *et al.* (Rabczuk *et al.* 2004, 2007, 2010) have proposed a theoretical approach for modeling discrete cracks in the framework of the meshfree method. In these approaches, the crack was represented as a collection of cracked particles, and a discontinuity along a plane was introduced to the failure direction at each cracked particle (Rabczuk *et al.* 2004, 2007). They reported that their theoretical approach enables the modeling of the nucleation of cracks and complex patterns involving crack branching and crossing (Rabczuk *et al.* 2004, 2007). However, the present simulation used the CDP model to consider the irreversible damage that happened during the fracturing procedure without considering the effects of the damage evolution and crack propagation by the discrete cracks. It should, thus, be noted that the present simulation did not consider the effect of the damage evolution and crack propagation by discrete cracks in concrete.

The specimens were modeled using an eight-node reduced integration solid element. A two-node linear truss element was applied to simulate the rebars and the stirrups in the RC beam (Park *et al.* 2017). Fig. 11 shows the simulated load-displacement behaviors of control specimens to different global mesh sizes. Each size of the dataset of 5, 15, and 20 global mesh sizes, which are composed of the load-displacement behaviors, is 123, 30, and 18 in the range of a displacement of 1 - 5 mm, respectively. The load values of all mesh sizes converge to approximately 21 kN at a displacement of 5 mm, though the load value of the 20 mesh size is slightly lower compared to the other mesh sizes due to the insufficient dataset at a displacement of 1 mm. Hence, the mesh size in the present simulations is determined to be the 15 global mesh size based on the results in Fig. 11 due to the computational limitations in considering a huge number of elements in the 5 global mesh size.

The E-series specimens with a commercially available adhesive were assumed to exhibit perfect bonding between the RC beam and the UHPC panel given that the interfacial area showed proper compatibility until the peak strength of the specimen was reached in the experimental results. Meanwhile, the interfacial bond characteristics of the I-series specimens were assumed to have two types of interactions: tangential and normal behavior. To apply the tangential behavior to the I-series specimens, the friction value between the RC beam and the UHPC panel was estimated to be 0.6, as provided in Eurocode 2 (CEN 2004, Hussein *et al.* 2016, Jeon *et al* 2022), and the hard contact condition was assumed to simulate the normal behavior.

The experimentally and simulated load-displacement behaviors of the RC beam strengthened with the UHPC panel are displayed in Fig. 12. The simulated flexural behavior of I30, I50, and I70 specimens showed in fair agreement with the experimental results as shown in Fig. 12 (b). The simulated initial stiffness of the I10 specimen was predicted to be lower than that from the experimental results in an early elastic range, resulting in a lower peak in the finite element simulation in comparison with the obtained failure load in the experiment (Kim *et al* 2018). This discrepancy is likely due to the adhesion of the UHPC panel. A sudden reduction in the stiffness of the experimental result was observed just after beyond displacement of 1 mm. That is, the adhesion of the UHPC panel affected the increase in stiffness at early loading stage up to the displacement of 1 mm.

The predicted stiffness and peak strength of the E-series specimens were improved with an increase in the thickness

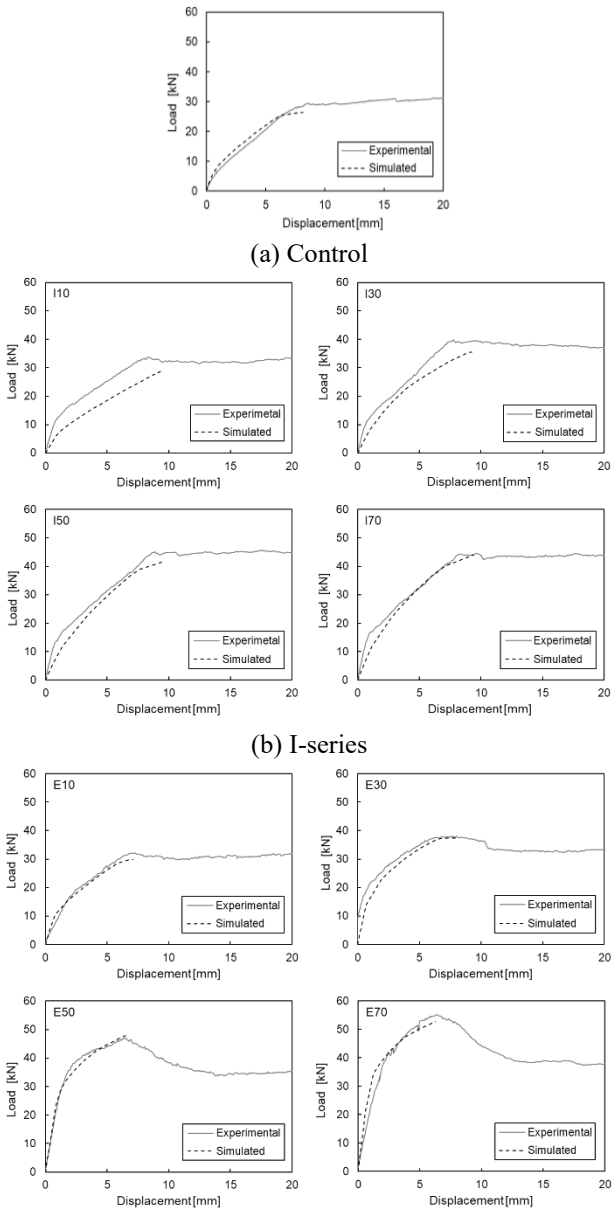

(a) Control

(b) I-series

(c) E-series

Fig. 12 Experimentally and simulated load-displacement behaviors (a) Control, (b) I-series and (c) E-series specimens (Solid and Dotted lines indicate experimental and simulated load-displacement curve, respectively.)

of the UHPC panel. In particular, the E30, E50, and E70 specimens showed noticeable increases in the stiffness and peak strength, while both the experimental and simulated results for the E10 specimen showed flexural behavior, similar to those of the control specimen (Fig. 12(a)). However, the observed difference from the experiment after the peak strength in E30, E50, and E70 specimens may be due to the simulation presumption that the RC beam and the UHPC panel was perfectly bonded each other, in which failure mode such as debonding of the UHPC panel from the RC beam was not considered (Cai *et al.* 2020).

The illustrations of the deformed shape with the displacement of y-direction and von-Mises effective stress

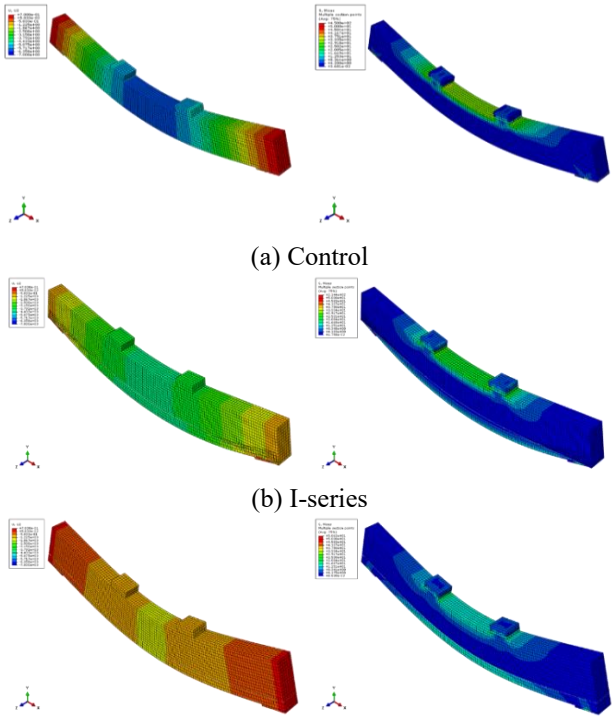

(a) Control

(b) I-series

(c) E-series

Fig. 13 Deformed shape with the displacement of y-direction and von-Mises effective stress of the (a) Control, (b) I50 and (c) E50 specimens

of the control, I50, and E50 specimens under a four-point loading are shown in Fig. 13. These illustrations were simulated by virtually imposing a load of 25 kN in order to identify the flexural behavior of the specimens in the elastic region (Jang *et al* 2019). The displacement in the y-direction of the E50 specimen was much lower than that of the control and I50 specimens, which is in line with the experimental results. As indicated by the contour appeared on the UHPC panel, the E50 specimen displayed high von-Mises effective stress at the UHPC panel, showing that the UHPC panel of E50 specimen was able to distribute the stress effectively in the RC beam.

5. Conclusions

The present study investigated the flexural behavior of RC beams strengthened with UHPC panels of various thicknesses. The RC beams were strengthened using two methods: (1) direct casting of the UHPC (I-series), and (2) by attaching a UHPC panel using an adhesive onto the bottom surface of the RC beam (E-series). The flexural behavior the RC beam strengthened with UHPC was evaluated in terms of the failure mode and crack pattern, the load-deflection behavior, and the ductility in partnership with numerical analysis. The findings obtained from this study are given below.

- The propagation and growth of cracks on the surfaces of the RC beams strengthened with a UHPC panel were delayed, while the peak strength and energy dissipation

were improved in comparison with the control specimen. In addition, the strengthening effect increased proportionally with an increase in the thickness of the UHPC panel regardless of the strengthening method used.

• The strengthening effect of the UHPC panel on the I- and E-series specimens was comparable when the thickness of the UHPC panel was 10 mm and 30 mm. However, the E50 and E70 specimens showed more enhanced strengthening performance compared to the I50 and I70 specimens, this is attributed to the bonding characteristics between the RC beam and the UHPC panel.

• The predictions calculated from a numerical analysis were in good agreement with the experimental results. Although the prediction of the stiffness of a few specimens showed some extent of discrepancy due to difficulties in defining the bonding properties in these specimens, the simulated load-deflection of the RC beam strengthened with a UHPC panel showed high similarity with the experimental results.

The present paper specifically examined the flexural behavior of reinforced concrete beams strengthened UHPC panels of various thicknesses. It should, thus, be noted that the present experiments and simulations are designed to investigate the flexural behavior of RC concrete beams strengthened UHPC panels without the other failure mechanisms such as shear failure and anchorage failure. Therefore, relevant experimental schemes capable of considering the other failure mechanisms can be performed for any forthcoming studies.

Acknowledgment

This work was supported by the National Research Foundation of Korea grant funded by the Korean government (MSIT) (2020R1C1C1005063).

References

ABAQUS (2013), 6.13 Analysis User's Manual, SIMULIA, Providence, IR, USA.

Al-Osta, M., Isa, M., Baluch, M. and Rahman, M. (2017), "Flexural behavior of reinforced concrete beams strengthened with ultra-high performance fiber reinforced concrete", *Constr. Build. Mater.*, **134**, 279-296. https://doi.org/10.1016/j.conbuildmat.2016.12.094.

ASTM-C143 (2015), Standard Test Method for Slump of Hydraulic-Cement Concrete, ASTM International, West Conshohocken, PA, USA.

ASTM-C1437 (2020), Standard Test Method for Flow of Hydraulic Cement Mortar, ASTM International, West Conshohocken, PA, USA.

ASTM-C348 (2021), Standard Test Method for Flrexural Strength of Hydraulic-Cement Mortars, ASTM International, West Conshohocken, PA, USA.

ASTM-C39/C39M (2021), Standard Test Method Compressive Strength of Cylindrical Concrete Specimens, ASTM International, West Conshohocken, PA, USA.

ASTM-C469 (2021), Standard Test Method for Static Modulus of Elasticity and Poisson's Ratio of Concrete in Compression, ASTM International, West Conshohocken, PA, USA.

ASTM-C496 (2021), Standard Test Method for Splitting Tensile Strength of Cylindrical Concrete Specimens, ASTM International, West Conshohocken, PA, USA.

ASTM C496-96 (2017), Standard Test Method for Splitting Tensile Strength of Cylindrical Concrete Specimens, ASTM International, West Conshohocken, PA, USA.

Attari, N., Amziane, S. and Chemrouk, M. (2012), "Flexural strengthening of concrete beams using CFRP, GFRP and hybrid FRP sheets", *Constr. Build. Mater.*, **37**, 746-757. https://doi.org/10.1016/j.conbuildmat.2012.07.052.

Bang, J., Bae, J.H., Jung, J. and Yang, B. (2022), "A Short review of the literature on the multiscale modeling of nanoparticle-reinforced composites", *Multiscale Sci. Eng.*, **4**(3), 94-101. https://doi.org/10.1007/s42493-022-00083-y.

Buyukozturk, O. and Hearing, B. (1998), "Failure behavior of precracked concrete beams retrofitted with FRP", *J. Compos. Constr.*, **2**(3), 138-144. https://doi.org/10.1061/(ASCE)1090-0268(1998)2:3(138).

Cai, B., Wu, A. and Fu, F. (2020), "Bond behavior of PP fiber-reinforced cinder concrete after fire exposure", *Comput. Concrete*, **26**(2), 115-125. https://doi.org/10.12989/cac.2020.26.2.115.

CEN (2004), 1-1. Eurocode 2: Design of concrete structures-Part 1-1: General rules and rules for buildings, European Committee for Standardization, Brussels, Belgium.

Choi, S.H., Heo, I., Kim, J.H., Jeong, H., Lee, J.Y. and Kim, K.S. (2022), "Flexural behavior of post-tensioned precast concrete girder at negative moment region", *Comput. Concrete*, **30**(1), 75-83. https://doi.org/10.12989/cac.2022.30.1.075.

Deng, Z. (2005), "The fracture and fatigue performance in flexure of carbon fiber reinforced concrete", *Cement Concrete Compos.*, **27**(1), 131-140. https://doi.org/10.1016/j.cemconcomp.2004.03.002.

El-Enein, H.A., Azimi, H., Sennah, K. and Ghrib, F. (2014), "Flexural strengthening of reinforced concrete slab-column connection using CFRP sheets", *Constr. Build. Mater.*, **57**, 126-137. https://doi.org/10.1016/j.conbuildmat.2014.01.077.

El-Mihilmy, M.T. and Tedesco, J.W. (2000), "Analysis of reinforced concrete beams strengthened with FRP laminates", *J. Struct. Eng.*, **126**(6), 684-691. https://doi.org/10.1061/(ASCE)0733-9445(2000)126:6(684).

Gil-Martina, L.M. and Hernandez-Montes, E. (2021), "Review of the reinforcement sizing in the strength design of reinforced concrete slabs", *Comput. Concrete*, **27**(3), 211-223. https://doi.org/10.12989/cac.2021.27.3.211.

Haile, B.F., Jin, D., Yang, B., Park, S. and Lee, H.K. (2019), "Multi-level homogenization for the prediction of the mechanical properties of ultra-high-performance concrete", *Constr. Build. Mater.*, **229**, 116797. https://doi.org/10.1016/j.conbuildmat.2019.116797.

Hamdia, K.M., Silani, M, Zhuang, X., He, P. and Rabczuk, T. (2017), "Stochastic analysis of the fracture toughness of polymeric nanoparticle composites using polynomial chaos expansions", *Int. J. Fract.*, **206**, 215-227. https://doi.org/10.1007/s10704-017-0210-6.

Hussein, H.H., Walsh, K.K., Sargand, S.M. and Steinberg, E.P. (2016), "Interfacial properties of ultrahigh-performance concrete and high-strength concrete bridge connections", *J. Mater. Civil Eng.*, **28**(5), 04015208. https://doi.org/10.1061/(ASCE)MT.1943-5533.0001456.

Hussein, L. and Amleh, L. (2015), "Structural behavior of ultra-high performance fiber reinforced concrete-normal strength concrete or high strength concrete composite members", *Constr. Build. Mater.*, **93**, 1105-1116. https://doi.org/10.1016/j.conbuildmat.2015.05.030.

Jang, H.G., Yang, B., Khil, M.S., Kim, S.Y. and Kim, J. (2019), "Comprehensive study of effects of filler length on mechanical, electrical, and thermal properties of multi-walled carbon nanotube/polyamide 6 composites", *Compos. Part A: Appl. Sci. Manuf.*, **125**, 105542. https://doi.org/10.1016/j.compositesa.2019.105542.

Jeon, I., Yun, T. and Yang, S. (2022), "Classical, coarse-grained, and reactive molecular dynamics simulations on polymer nanocomposites", *Multiscale Sci. Eng.*, **4**(4), 1-18. https://doi.org/10.1007/s42493-022-00086-9.

Kassem, C., Farghaly, A.S. and Benmokrane, B. (2011), "Evaluation of flexural behavior and serviceability performance of concrete beams reinforced with FRP bars", *J. Compos. Constr.*, **15**(5), 682-695. https://doi.org/10.1061/(ASCE)CC.1943-5614.0000216.

Kim, K., Jung, Y.C., Kim, S.Y., Yang, B.J. and Kim, J. (2018), "Adhesion enhancement and damage protection for carbon fiber-reinforced polymer (CFRP) composites via silica particle coating", *Compos. Part A: Appl. Sci. Manuf.*, **109**, 105-114. https://doi.org/10.1016/j.compositesa.2018.02.042.

Lee, H.K. and Hausmann, L. (2004), "Structural repair and strengthening of damaged RC beams with sprayed FRP", *Compos. Struct.*, **63**(2), 201-209. https://doi.org/10.1016/S0263-8223(03)00156-9.

Lee, J. and Fenves, G.L. (1998), "Plastic-damage model for cyclic loading of concrete structures", *J. Eng. Mech.*, **124**(8), 892-900. https://doi.org/10.1061/(ASCE)0733-9399(1998)124:8(892).

Lee, N.K., Koh, K., Kim, M.O. and Ryu, G. (2018), "Uncovering the role of micro silica in hydration of ultra-high performance concrete (UHPC)", *Cement Concrete Res.*, **104**, 68-79. https://doi.org/10.1016/j.cemconres.2017.11.002.

Lubbers, A.R. (2003), "Bond performance between ultra-high performance concrete and prestressing strands", Doctoral Dissertation, Ohio University, Athens, OH, USA.

Lubliner, J., Oliver, J., Oller, S. and Oñate, E. (1989), "A plastic-damage model for concrete", *Int. J. Solid. Struct.*, **25**(3), 299-326. https://doi.org/10.1016/0020-7683(89)90050-4.

Manfredi, G. and Pecce, M. (1997), "Low cycle fatigue of RC beams in NSC and HSC", *Eng. Struct.*, **19**(3), 217-223. https://doi.org/10.1016/S0141-0296(96)00081-8.

Monti, G. and Liotta, M.A. (2005), "FRP-strengthening in shear: Tests and design equations", *Spec. Publ.*, **230**, 543-562. https://doi.org/10.14359/14853.

Murthy, A.R., Karihaloo, B.L. and Priya, D.S. (2018b), "Flexural behavior of RC beams retrofitted with ultra-high strength concrete", *Constr. Build. Mater.*, **175**, 815-824. https://doi.org/10.1016/j.conbuildmat.2018.04.174.

Murthy, A.R., Karihaloo, B.L., Rani, P.V. and Priya, D.S. (2018a), "Fatigue behaviour of damaged RC beams strengthened with ultra high performance fibre reinforced concrete", *Int. J. Fatigue*, **116**, 659-668. https://doi.org/10.1016/j.ijfatigue.2018.06.046.

Park, S., Yang, B., Kim, B., Ha, S. and Lee, H. (2017), "Structural strengthening and damage behaviors of hybrid sprayed fiber-reinforced polymer composites containing carbon fiber cores", *Int. J. Damage Mech.*, **26**(2), 358-376. https://doi.org/10.1177/1056789516673887.

Rabczuk, T. and Belytschko, T. (2007), "A three-dimensional large deformation meshfree method for arbitrary evolving cracks", *Comput. Method Appl. M.*, **196**(29-30), 2777-2799. https://doi.org/10.1016/j.cma.2006.06.020.

Rabczuk, T. and Belytschko, T. (2004), "Cracking particles: A simplified meshfree method for arbitrary evolving cracks", *Int. J. Numer. Meth. Eng.*, **61**(13), 2316-2343. https://doi.org/10.1002/nme.1151.

Rabczuk, T., Zi, G., Bordas, S. and Nguyen-Xuan, H. (2008), "A geometrically non-linear three-dimensional cohesive crack method for reinforced concrete structures", *Eng. Fract. Mech.*, **75**(16), 4740-4758. https://doi.org/10.1016/j.engfracmech.2008.06.019.

Rabczuk, T., Zi, G., Bordas, S. and Nguyen-Xuan, H. (2010), "A simple and robust three-dimensional cracking-particle method without enrichment", *Comput. Method Appl. M.*, **199**(37-40), 2437-2455. https://doi.org/10.1016/j.cma.2010.03.031.

Spadea, G., Bencardino, F. and Swamy, R.N. (1998), "Structural behavior of composite RC beams with externally bonded CFRP", *J. Compos. Constr.*, **2**(3), 132-137. https://doi.org/10.1061/(ASCE)1090-0268(1998)2:3(132).

Theriault, M. and Benmokrane, B. (1998), "Effects of FRP reinforcement ratio and concrete strength on flexural behavior of concrete beams", *J. Compos. Constr.*, **2**(1), 7-16. https://doi.org/10.1061/(ASCE)1090-0268(1998)2:1(7).

Toutanji, H., Zhao, L. and Zhang, Y. (2006), "Flexural behavior of reinforced concrete beams externally strengthened with CFRP sheets bonded with an inorganic matrix", *Eng. Struct.*, **28**(4), 557-566. https://doi.org/10.1016/j.engstruct.2005.09.011.

Wenwei, W. and Guo, L. (2006), "Experimental study and analysis of RC beams strengthened with CFRP laminates under sustaining load", *Int. J. Solids Struct.*, **43**(6), 1372-1387. https://doi.org/10.1016/j.ijsolstr.2005.03.076.

Yalçınkaya, Ç. and Yazıcı, H. (2017), "Effects of ambient temperature and relative humidity on early-age shrinkage of UHPC with high-volume mineral admixtures", *Constr. Build. Mater.*, **144**, 252-259. https://doi.org/10.1016/j.conbuildmat.2017.03.198.

CC